Available online at www.sciencedirect.com

ScienceDirect

journal homepage: www.elsevier.com/locate/he

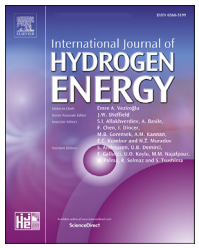

Short Communication

First-principles investigation of $BiVO_3$ for thermochemical water splitting

Marc Ong [a], *Quinn Campbell* [b,c,*], *Ismaila Dabo* [b,c], *Radi A. Jishi* [a]

[a] *Department of Physics and Astronomy, California State University, Los Angeles, Los Angeles, CA 90032, USA*
[b] *Department of Materials Science and Engineering, The Pennsylvania State University, University Park, PA 16802, USA*
[c] *Materials Research Institute, The Pennsylvania State University, University Park, PA 16802, USA*

ARTICLE INFO

Article history:
Received 20 August 2018
Received in revised form
30 October 2018
Accepted 15 November 2018
Available online 12 December 2018

Keywords:
Thermochemical water splitting
$BiVO_3$
First principles
Thermodynamics
Hydrogen

ABSTRACT

Thermochemical water splitting is a promising clean method of hydrogen production of high relevance in a society heavily reliant on fossil fuels. Using evolutionary methods and density functional theory, we predict the structure and electronic properties of $BiVO_3$. We build on previous literature to develop a framework to evaluate the thermodynamics of thermochemical water splitting cycles for hydrogen production. We use these results to consider the feasibility of $BiVO_3$ as a catalyst for thermochemical water splitting. We show that for $BiVO_3$, both the thermal reduction and gas splitting reactions are thermodynamically favorable under typical temperature conditions. We predict that thermochemical water splitting cycles employing $BiVO_3$ as a catalyst produce hydrogen yields comparable to those of commonly used catalysts.

Introduction

Many aspects of modern society depend on the production and use of chemical fuels. Hydrogen gas is a promising alternative to conventional modern-day fuels, as its combustion only produces water as a byproduct. Hydrogen is usually produced by steam reforming reactions with fossil fuels at high temperatures; however, these processes generate carbon dioxide and other greenhouse gases, motivating the search for other methods of hydrogen generation [7].

Alternative methods for hydrogen production have been explored. Thermochemical water splitting cycles have high theoretical solar-to-fuel conversion efficiencies, due to their ability to utilize the entire solar spectrum [34]. Efficiencies are projected to be higher than in other methods, such as photocatalysis and photovoltaic-driven electrolysis [13,33]. In the simplest thermochemical water splitting process, a cycle consists of two steps: thermal reduction (TR) followed by gas splitting (GS), and it employs a metal oxide as a catalyst. In the TR step, solar energy is concentrated to heat a metal oxide to a

* *Corresponding author*. Department of Materials Science and Engineering, The Pennsylvania State University, University Park, PA 16802, USA.
E-mail address: quinn.campbell@psu.edu (Q. Campbell).
https://doi.org/10.1016/j.ijhydene.2018.11.125
0360-3199/

thermal reduction temperature T_{TR} at which oxygen vacancies are produced:

$$MO_x \rightarrow MO_{x-\delta} + \frac{\delta}{2}O_2 \quad (1)$$

In the GS step, carried out at a lower temperature T_{GS}, the reaction of the reduced metal oxide with steam produces hydrogen gas and regenerates the catalyst:

$$MO_{x-\delta} + \delta H_2O \rightarrow MO_x + \delta H_2 \quad (2)$$

Analogous schemes have been explored for the splitting of CO_2 into CO and O_2 [34]. Many binary metal oxides, such as ZnO [25,35], Fe_3O_4 [14], and CeO_2 [1,6,30] have been studied for the purpose of thermochemical water splitting. Among the most successful was CeO_2, which is regarded as the benchmark for the performance of other catalysts, due to fast kinetics and robustness to phase changes in the presence of high amounts of oxygen vacancies [6,31]. However, CeO_2 demands a high TR temperature (around 2000 °C) to produce reasonable amounts of hydrogen fuel [40], making practical implementation difficult. Additionally, there are concerns of sublimation of this compound at high temperatures [10].

Recently, perovskite metal oxides have been proposed as promising materials for thermochemical water splitting [23]. These materials require lower temperatures for thermal reduction than binary metal oxides, and are resistant to structural changes in the case of high oxygen off-stoichiometry [8]. For instance, it has been shown that doped lanthanum aluminate catalysts have outperformed ceria under certain conditions [23], and other types of lanthanum perovskites, such as strontium-doped lanthanum manganates, have been explored due to promising experimental results [3,32,40].

Many different metal oxide perovskites exist with a diverse array of elements. Such variety opens the door for tuning of the catalytic properties of this class of materials. In a recent study by Emery et al. [8], a high-throughput density-functional theory (HT–DFT) approach was used to explore 5329 different ABO_3-type perovskites. Many different compounds were screened to determine their chemical stability and the energy cost of forming an oxygen vacancy. The study identified many potentially stable perovskite oxides with vacancy formation energies close to the corresponding value in CeO_2.

In this paper, we present density functional theory calculations on the perovskite $BiVO_3$ and consider its use as a catalyst in water splitting processes. We use an evolutionary method to predict its most stable structure and determine its electronic properties. We then construct a supercell and calculate the oxygen vacancy formation energy. We present a thermodynamic framework that allows us to investigate the favorability of thermal reduction and gas splitting reactions when $BiVO_3$ is used as a catalyst.

Methods

Prediction of the crystal structure of $BiVO_3$ was performed using evolutionary methods, as implemented in two different codes, USPEX and CALYPSO. The USPEX code, developed by Oganov et al. [22,28,29], features local structure optimization, real-space representation and variational operators that mimic natural evolution. In the CALYPSO code [38], the structures are updated using the particle swarm optimization method.

In both codes, the evolutionary search is initialized by generating a population of structures with randomly selected space groups. Using density functional theory (DFT), each structure is optimized and its total energy (known as the fitness function) calculated. Both codes were linked to the Vienna *ab-initio* Simulation Package (VASP) [16–19], which uses the projector augmented wave method with a plane wave basis set, to perform the DFT calculations. The optimization is performed in four steps, beginning with a coarse optimization that turns gradually finer. In the final step, the kinetic energy cutoff for the plane-wave expansion is 600 eV. The optimized structures thus obtained form the first generation. A new generation is now produced, some members of which are generated randomly, while the rest descend from the best structures (those with lowest energy) of the previous generation. In USPEX, new structures (offspring) are generated from parent structures by applying variational operators such as heredity, mutation, or permutation. In CALYPSO, an evolutionary algorithm is used to update the atomic positions in order to produce new structures. The structures in the new generation are optimized, and the best among them are used to produce the next generation. The process continues until convergence to the best structures is attained.

The density of states of the most stable structure of $BiVO_3$ was determined using the all-electron, full-potential, linearized, augmented plane wave method implemented in the WIEN2k code [2]. Here, two regions of space are considered. The interior region consists of non-overlapping muffin-tin spheres centered on each atom in the unit cell, while the interstitial region consists of the space between the spheres. The electronic wave function is expanded in a basis set of functions which assume different forms in different regions. Within a muffin-tin sphere, they are atomic-like functions expanded in spherical harmonics up to $\ell_{max}=10$. In the interstitial, they are plane waves, with a maximum wave vector magnitude of k_{max}, such that $R_{mt}k_{max}=8$, where R_{mt} is the radius of the smallest muffin-tin sphere in the unit cell. The charge density was expanded as a Fourier series with a maximum wave vector of $14/a_0$, with a_0 as the Bohr radius. Self-consistent field (SCF) calculations were performed until energy convergence of 10^{-4} Ry and charge convergence of 10^{-3} e are achieved. For the vanadium ion, a Hubbard on-site Coulomb term, U=4 eV, and Hund's exchange term, J=0.7 eV, were used. Spin orbit coupling (SOC) effects were included in the calculation because of the presence of Bi, which has a large atomic number. The modified Becke–Johnson (mBJ) exchange potential [37] was adopted in our calculations; this is known to produce accurate band gap values in semiconductors [15].

The oxygen vacancy formation energy ΔE_v^O is the energy change upon removal of a single oxygen atom from the bulk crystal. It is defined as follows:

$$\Delta E_v^O = \frac{1}{\delta}\left(E_{ABO_{3-\delta}} - E_{ABO_3}\right) - \mu_O \quad (3)$$

where δ is the oxygen off-stoichiometry ($\delta \ll 1$), $E_{ABO3-\delta}$ is the total energy of the crystal with vacancies, E_{ABO3} is the total

energy of the perfect crystal, and μ_O is the chemical potential of an oxygen atom. Ideally, ΔE_v^O should converge as larger supercells are used and δ approaches zero.

In calculating the oxygen vacancy formation energy, it is assumed that the vacancy is neutral, as implied in (3). In some crystals, such as ZnO [21] and ZrO_2 [42], the oxygen vacancy can be doubly charged, and thus inducing *n*-type conductivity via a self doping effect. However, in other materials, such as CeO_2 [27], the oxygen vacancy is neutral; the extraction of an oxygen atom is accompanied by the reduction of two neighboring Ce(IV) ions to Ce(III) ions. A similar situation occurs in V_2O_5 [39], where vanadium ions in the vicinity of the vacancy are reduced from V^{+5} to V^{+4} or even V^{+3}.

Oxygen vacancy formation energy was calculated by obtaining the total energy within DFT + *U* after optimizing a 2×2×2 supercell missing one oxygen atom and comparing it to the energy of the bulk material. The values of *U* and *J* are the same as given earlier. Because one oxygen atom was removed out of the 96 total in the supercell, δ=1/32 in our case, which is sufficiently small that it is expected to yield an accurate result for the oxygen vacancy formation energy.

Crystal structure and electronic properties

The results of the evolutionary search are listed in Table 1, which shows the predicted crystal structures of $BiVO_3$ with lowest energies. The most stable structure is orthorhombic with space group *Pnma* (number 62). We have considered different magnetic structures and found that the ground state is ferromagnetic with a magnetic moment on each V ion given by $1.97\mu_B$, where μ_B is the Bohr magneton. The *A*-type antiferromagnetic structure has an energy of 2 meV per formula unit higher than the ferromagnetic structure. The *G*-type and *C*-type antiferromagnetic structures have energies slightly higher than the *A*-type structure. Structures with space groups 7, 29, and 161 lack inversion symmetry, and may be of interest for further study as possible multiferroic materials.

The calculated electronic density of states is shown in Fig. 1. From this plot, we obtain a band gap of 2.4 eV for the orthorhombic phase of $BiVO_3$. The states near the conduction band minimum are primarily contributed by V *d*-orbitals, while the valence band maximum is mainly comprised of O *p*-orbitals. We provide these electronic structure calculations in the hope that it would be useful for future work regarding the effect of vacancies on the electronic properties of this crystal and the localized states those vacancies may form in the gap.

Table 1 – Table of crystal structures with lowest energy found by evolutionary search. The energy of the most stable structure is set to zero for ease of comparison.

Space group	Lattice constants (Å) and angles (degrees)	Energy (eV/atom)
62	a=5.494,b=5.787,c=7.909;α=β=γ=90	0.000
7	a=5.711,b=8.011,c=18.057;α=γ=90,β=18.439	0.014
29	a=3.263,b=7.513,c=10.263;α=β=γ=90	0.042
60	a=3.253,b=7.499,c=10.253;α=β=γ=90	0.043
161	a=b=c=5.708;α=β=γ=59.344	0.085

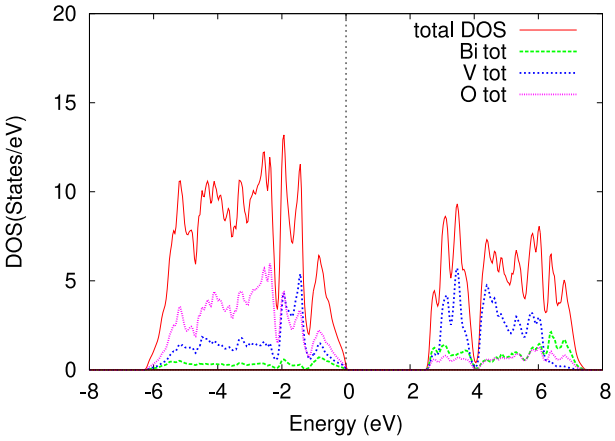

Fig. 1 – Electronic density of states for $BiVO_3$.

Thermodynamics

For $BiVO_3$ to be a viable candidate as a catalyst for thermochemical water splitting, both the thermal reduction and gas splitting reactions should be thermodynamically favorable, i.e., have negative free energies. In addition to the gases present in the reaction, the free energy is affected by the oxygen vacancy formation energy, as well as vibrational and configurational entropy changes.

Previous studies [24] have suggested frameworks to assess the thermodynamics of both the TR and GS reactions of water splitting cycles. However, analysis has focused specifically on binary metal oxides with perfectly stoichiometric reactions. It is difficult for such stoichiometric reactions to be thermodynamically favorable. For instance, in order for TR and GS reactions to result in a negative free energy change at typical temperatures for experiments, the entropy change in the reduction reaction must be large and positive. This is hard to achieve, as the stoichiometrically reduced material has significantly less vibrational degrees of freedom. Because of this, most of the oxides investigated seemed to have thermodynamically unfavorable properties, despite their apparent successes in experimental work.

In our analysis, the reactions are taken to be non-stoichiometric. We assume that the number of oxygen vacancies formed in the thermal reduction step is equal to the number produced at equilibrium, and is small compared to the total number of oxygen atoms in the crystal. Because the system is in equilibrium after the thermal reduction step, the free energy is minimized. Hence, in our framework, any arbitrary temperature of thermal reduction, T_{TR}, is allowed. Based on this, we evaluate the temperature T_{GS} required for the gas splitting step to be thermodynamically favorable given a particular T_{TR}.

Using the methods described in Section Methods, the oxygen vacancy formation energy obtained was 3.72 eV, comparable to the values observed in CeO_2 [5,26,41]. With this energy in hand, we can examine the thermal reduction: after heating a large crystal of $BiVO_3$ containing *N* oxygen atoms, *M* oxygen atoms are liberated. The chemical reaction in this step is thus

$$\frac{N}{3}BiVO_3 \rightarrow \frac{N}{3}BiVO_{3-\frac{3M}{N}} + \frac{M}{2}O_2 \quad (4)$$

The free energy ΔG_{TR} of this reaction at a temperature T_{TR} is given by

$$\Delta G_{TR} = M\Delta E_v^O - T_{TR}\left(\Delta S_{red,T_{TR}} + \frac{M}{2}S_{O_2,T_{TR}}\right) \quad (5)$$

Here, ΔE_v^O is the oxygen vacancy formation energy, T_{TR} is the thermal reduction temperature, $S_{O_2,T_{TR}}$ is the standard-state entropy of formation for O_2, and $\Delta S_{red,T_{TR}}$ is the entropy change of the reduction of the crystal at a temperature T_{TR}. This term can be calculated as the sum of the contribution from vibrational entropy change (ΔS_v) and configurational entropy change (ΔS_c).

Enthalpies and entropies of formation for O_2, H_2, and H_2O were taken from NIST-JANAF experimental fits of the Shomate equation [4], which is given by

$$\Delta H_f = AT + \frac{1}{2}BT^2 + \frac{1}{3}CT^3 + \frac{1}{4}DT^4 - \frac{E}{T} + F \quad (6)$$

and

$$S = A\ln(T) + BT + \frac{1}{2}CT^2 + \frac{1}{3}DT^3 - \frac{E}{2T^2} + G \quad (7)$$

where ΔH_f is the standard-state enthalpy of formation, S is the standard-state entropy of formation, T is temperature and A,B,C,D,E,F, and G are empirically determined piecewise constants. For a system of N harmonic oscillators, the vibrational entropy [9] is

$$S_v = 3Nk + k\sum_{i=1}^{3N}\ln\left(\frac{kT}{\hbar\omega_i}\right) \quad (8)$$

where S_v is the vibrational entropy, k is Boltzmann's constant, T is temperature, $\hbar$ is the reduced Planck constant, and ω_i is the angular frequency of the ith mode. Since a calculation of the vibrational frequencies of the supercell with a vacancy is unrealistic, we here adopt the simplified Einstein model in which all the atoms vibrate with the same frequency ω. This approach is widely used in calculating vacancy thermodynamics in perovskite oxides [20,36]. Hence, we write

$$S_v = 3Nk\left[\ln\left(\frac{kT}{\hbar\omega}\right) + 1\right] \quad (9)$$

If M oxygen atoms are now removed from the system, the total number of modes should be reduced to $3N-3M$. If we assume that the vibrational frequencies are unaffected except at the positions neighboring the vacancies, the new vibrational entropy S_v' is

$$S_v' = (3N-3M)k + (3N-3M-3MZ)k\ln\left(\frac{kT}{\hbar\omega}\right) + 3MZk\ln\left(\frac{kT}{\hbar\omega'}\right) \quad (10)$$

Here, Z is the number of neighbors to an oxygen atom in the crystal, and ω' is the modified frequency for the atoms neighboring the vacancies. (In this crystal, each oxygen atom has a coordination number of 2, with two neighboring vanadium atoms at 2.06 Å and 2.10 Å.) We estimate the modified frequency as

$$\omega' = \omega\sqrt{\frac{Z-1}{Z}} \quad (11)$$

The vibrational entropy change ΔS_v is the difference between the new and original vibrational entropies:

$$\Delta S_v = S_v' - S_v = -3Mk\left[1 + \ln\left(\frac{kT}{\hbar\omega}\right)\right] + 3MZk\ln\left(\frac{\omega}{\omega'}\right) \quad (12)$$

To obtain an estimate for ω, we calculated phonon frequencies at the Γ-point using Quantum ESPRESSO [11,12], and found frequencies ranging from 0 to 506 cm^{-1}, corresponding to approximately 0–720 K. As an intermediate value for the frequency, we choose $\hbar\omega/k$ to be 360 K.

The configurational entropy change ΔS_c is dictated by combinatorics:

$$\Delta S_c = k\ln\left[\frac{N!}{M!(N-M)!}\right] = kM\left[1 + \ln\left(\frac{N}{M}\right)\right] \quad (13)$$

The second equality results from using Stirling's approximation, in the limit that $N \gg M \gg 0$. At equilibrium, the fraction of oxygen vacancies that spontaneously form is obtained when ΔG is minimum, in other words, when $\partial\Delta G/\partial M = 0$. Substituting (13) into (5) and differentiating yields

$$\frac{M}{N} = \exp\left[-\frac{\Delta E_v^O - T\left(\Delta s_v + \frac{1}{2}S_{O_2,T}\right)}{kT}\right] \quad (14)$$

where $\Delta s_v = \Delta S_v/M$ is the vibrational entropy change per vacancy. This expression can be used to calculate the number of oxygen vacancies formed at a given thermal reduction temperature. The fraction of liberated atoms was estimated to be on the order of 10^{-14} at 1000 K, 10^{-8} at 1500 K, and 10^{-5} at 2000 K at atmospheric pressure.

Next, the GS step can be considered. If all of the M vacancies are filled, the chemical reaction is

$$\frac{N}{3}BiVO_{3-\frac{3M}{N}} + MH_2O \rightarrow \frac{N}{3}BiVO_3 + MH_2 \quad (15)$$

The free energy change ΔG_{GS} of this reaction carried out at a temperature T_{GS} is given by

$$\Delta G_{GS} = -M\Delta H_{f,H_2O,T_{GS}} - M\Delta E_v^O - T_{GS}\left(\Delta S_{ox,T_{GS}} + MS_{H_2,T_{GS}} - MS_{H_2O,T_{GS}}\right) \quad (16)$$

where $\Delta H_{f,H_2O,T_{GS}}$ is the standard-state enthalpy of formation of H_2O at temperature T_{GS}, $\Delta S_{ox,T_{GS}}$ is the entropy of oxidation of the crystal at temperature T_{GS}, $S_{H_2,T_{GS}}$ is the standard-state entropy of H_2 at temperature T_{GS}, and $S_{H_2O,T_{GS}}$ is the standard-state entropy of H_2O at temperature T_{GS}.

The entropy of oxidation, ΔS_{ox}, is given as

$$\Delta S_{ox,T_{GS}} = -\left(\Delta S_{v,T_{GS}} + \Delta S_c\right) \quad (17)$$

The configurational component does not change because the number of vacancies is fixed by the thermal reduction step, but the vibrational component changes, as it is temperature dependent.

T_{GS} should be chosen such that $\Delta G_{GS} \leq 0$. Because the Shomate equation for entropy contains both logarithm and polynomial terms in T_{GS}, we cannot write down a closed form expression for T_{GS} in terms of T_{TR}. Thus, we set (16) to be less

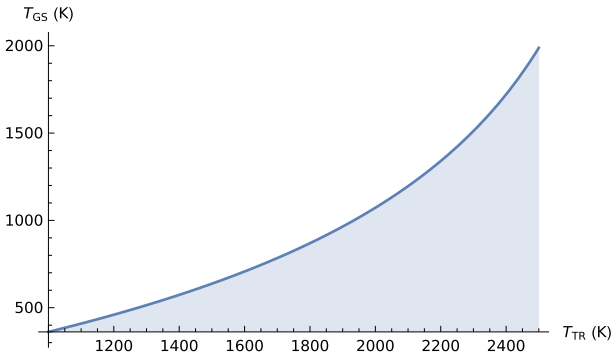

Fig. 2 – Plot of favorable temperatures T_{GS} for gas splitting reaction as a function of T_{TR}. The region below the blue line represents the set of temperatures at which both thermal reduction and gas splitting are thermodynamically favorable. (For interpretation of the references to color in this figure legend, the reader is referred to the Web version of this article.)

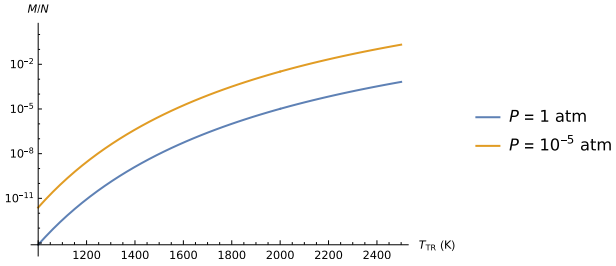

Fig. 3 – Plot of equilibrium fraction of oxygen vacancies as a function of T_{TR} at atmospheric pressure and at 10^{-5} atm.

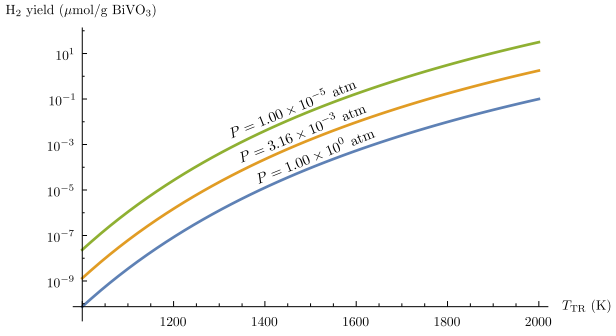

Fig. 4 – Plot of calculated hydrogen yield as a function of temperature, evaluated at three different pressures.

than or equal to zero and solve numerically for T_{GS}. Because the entropy of gas splitting is negative, the required T_{GS} is bounded above. In Fig. 2 we plot the upper bound of T_{GS} as a function of T_{TR}. The plot shows that T_{GS} is a reasonable number given standard values of T_{TR}. For instance, at 2000 K, the maximum value of T_{GS} is around 1072 K, which is around the typical temperature of 1000 K for gas splitting of previously tested compounds [24].

The fraction of oxygen vacancies that are formed at a given temperature can be increased by lowering the pressure at which thermal reduction is carried out. This can be calculated

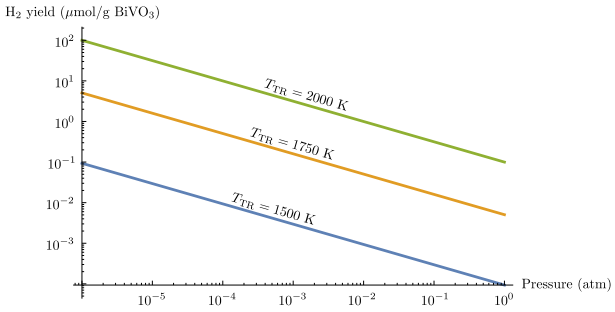

Fig. 5 – Plot of calculated hydrogen yield as a function of pressure, evaluated at three different temperatures.

by adding a correction of $-R\ln(P/P_0)$ to the standard-state entropy of O_2, where P_0 is the atmospheric pressure. This effect is illustrated in Fig. 3. For instance, if we decrease the pressure to 10^{-5} atm, a typical value for thermochemical water splitting [3], we obtain a value of M/N=3.2×10^{-3} at 2000 K, corresponding to a hydrogen production yield of 32 μmol per gram of the catalyst $BiVO_3$. This is of a similar order of magnitude compared to lanthanum-based perovskite catalysts [3]. We predict yields of 1.5 μmol/g and 0.03 μmol/g for values of T_{TR} given by 1750 K and 1500 K, respectively. The effects of temperature and pressure on the yield are shown in Figs. 4 and 5, respectively. As expected, the yield increases with an increase in temperature and a reduction in oxygen partial pressure.

Conclusion

In conclusion, we demonstrate that $BiVO_3$ may be of interest as a catalyst for thermochemical water splitting. We predict that using $BiVO_3$ as a catalyst for thermochemical water splitting can produce a promising hydrogen yield. Further work will be necessary to determine kinetics and other practical considerations of the application of this material in thermochemical water splitting.

Acknowledgements

M.O and R.J acknowledge support from the National Science Foundation under CREST grant no. HRD-1547723 and PREM grant no. DMR-1523588. Q.C. and I.D. acknowledge support from the National Science Foundation under CAREER grant no. DMR-1654625.

REFERENCES

[1] Abanades Stéphane, Flamant Gilles. Thermochemical hydrogen production from a two-step solar-driven water-splitting cycle based on cerium oxides. Sol Energy 2006;80:1611–23.

[2] Blaha P, Schwarz K, Madsen GKH, Kvasnicka D, Luitz J. WIEN2k, an augmented plane wave + local orbitals program for calculating crystal properties. Austria: Karlheinz Schwarz, Techn. Universität Wien; 2001. ISBN 3-9501031-1-2.

[3] Bork AH, Kubicek M, Struzik M, Rupp JLM. Perovskite $La_{0.6}Sr_{0.4}Cr_{1-x}Co_xO_{3-\delta}$ solid solutions for solar-thermochemical fuel production: strategies to lower the operation temperature. J Phys Chem 2015;(3):15546–57.

[4] Chase Jr MW. NIST-JANAF thermochemical tables 4th ed. J Phys Chem Ref Data 1998:1–1951. Monograph 9.

[5] Chiang Y-M, Lavik EB, Blom DA. Defect thermodynamics and electrical properties of nanocrystalline oxides: pure and doped CeO_2. Nanostruct Mater 1997;9(1):633–42. ISSN 0965-9773, https://doi.org/10.1016/S0965-9773(97)00142-6.

[6] Chueh William C, Falter Christoph, Abbott Mandy, Scipio Danien, Furler Philipp, Haile Sossina M, et al. High-flux solar-driven thermochemical dissociation of CO_2 and H_2O using nonstoichiometric ceria. Science 2010;330(6012):1797–801.

[7] Guido Collodi, Wheeler Foster. Hydrogen production via steam reforming with CO_2 capture. Chemical Engineering Transactions 2010;19:37–42.

[8] Emery Antoine A, Saal James E, Kirklin Scott, Hegde Vinay I, Wolverton Chris. High-throughput computational screening of perovskites for thermochemical water splitting applications. Chem Mater 2016;28(16):5621–34.

[9] Fultz Brent. Vibrational thermodynamics of materials. Prog Mater Sci 2010;55(4):247–352.

[10] Furler Philipp, Scheffe Jonathan R, Steinfeld Aldo. Syngas production by simultaneous splitting of H_2O and CO_2 via ceria redox reactions in a high-temperature solar reactor. Energy Environ Sci 2012;5(3):6098–103.

[11] Giannozzi P, Andreussi O, Brumme T, Bunau O, Buongiorno Nardelli M, Calandra M, et al. Advanced capabilities for materials modelling with quantum espresso. J Phys Condens Matter 2017;29(46):465901.

[12] Giannozzi Paolo, Baroni Stefano, Bonini Nicola, Calandra Matteo, Car Roberto, Cavazzoni Carlo, et al. Quantum espresso: a modular and open-source software project for quantum simulations of materials. J Phys Condens Matter 2009;21(39):395502.

[13] Kodama Tatsuya, Gokon Nobuyuki. Thermochemical cycles for high-temperature solar hydrogen production. Chem Rev 2007;107(10):4048–77.

[14] Tatsuya Kodama, Yumiko Nakamuro, and Takayuki Mizuno. A two-step thermochemical water splitting by iron-oxide on stabilized zirconia. J Sol Energy Eng, 128(1):3–7.

[15] Koller David, Tran Fabien, Blaha Peter. Merits and limits of the modified Becke-Johnson exchange potential. Phys Rev B 2011;83(19):195134.

[16] Kresse G, Furthmüller J. Efficiency of ab-initio total energy calculations for metals and semiconductors using a plane-wave basis set. Comput Mater Sci 1996;6(1):15–50.

[17] Kresse G, Furthmüller J. Efficient iterative schemes for ab initio total-energy calculations using a plane-wave basis set. Phys Rev B 1996;54(16):11169–86.

[18] Kresse G, Hafner J. Ab initio molecular dynamics for liquid metals. Phys Rev B 1993;47(1):558–61.

[19] Kresse G, Hafner J. Ab initio molecular-dynamics simulation of the liquid-metal amorphous-semiconductor transition in germanium. Phys Rev B 1994;49(20):14251–69.

[20] Lee Yueh-Lin, Morgan Dane, Kleis Jesper, Rossmeisl Jan. Ab initio defect energetics in $LaBO_3$ perovskite solid oxide fuel cell materials. ECS Trans 2009;25(2):2761–7.

[21] Liu Lishu, Mei Zengxia, Tang Aihua, Alexander Azarov, Kuznetsov Andrej, Xue Qi-Kun, et al. Oxygen vacancies: the origin of *n*-type conductivity in ZnO. Phys Rev B 2016;93(23):235305.

[22] Lyakhov Andriy O, Oganov Artem R, Stokes Harold T, Zhu Qiang. New developments in evolutionary structure prediction algorithm uspex. Comput Phys Commun 2013;184(4):1172–82.

[23] McDaniel Anthony H, Miller Elizabeth C, Arifin Darwin, Ambrosini Andrea, Coker Eric N, Ryan O'Hayre, et al. Sr- and Mn-doped $LaAlO_{3-\delta}$ for solar thermochemical H_2 and CO production. Energy Environ Sci 2013;6(8):2424–8.

[24] Meredig B, Wolverton C. First-principles thermodynamic framework for the evaluation of thermochemical H_2O- or CO_2-splitting materials. Phys Rev B 2009;80(24):245119.

[25] Müller R, Steinfeld A. H_2O-splitting thermochemical cycle based on ZnO/Zn-redox: quenching the effluents from the ZnO dissociation. Chem Eng Sci 2008;63(1):217–27.

[26] Murgida GE, Ferrari V, Verónica Ganduglia-Pirovano M, Llois AM. Ordering of oxygen vacancies and excess charge localization in bulk ceria: a DFT+*U* study. Phys Rev B 2014;90(11):115120.

[27] Nolan Michael, Parker Stephen C, Watson Graeme W. The electronic structure of oxygen vacancy defects at the low index surfaces of ceria. Surf Sci 2012;595(1–3):223–32.

[28] Oganov Artem R, Glass Colin W. Crystal structure prediction using ab initio evolutionary techniques: principles and applications. J Chem Phys 2006;124(24):244704.

[29] Oganov Artem R, Lyakhov Andriy O, Valle Mario. How evolutionary crystal structure prediction works—and why. Acc Chem Res 2011;44(3):227–37.

[30] Otsuka Kiyoshi, Hatano Masaharu, Morikawa Akira. Decomposition of water by cerium oxide of δ-phase. Inorg Chim Acta 1985;109(3):193–7.

[31] Perkins Christopher, Alan Weimer W. Solar -thermal production of renewable hydrogen. AIChE J 2009;55(2):286–93.

[32] Scheffe Jonathan R, Weibel David, Steinfeld Aldo. Lanthanum–strontium–manganese perovskites as redox materials for solar thermochemical splitting of H_2O and CO_2. Energy Fuels 2013;27(8):4250–7.

[33] Siegel Nathan P, Miller James E, Ermanoski Ivan, Diver Richard B, Stechel Ellen B. Factors affecting the efficiency of solar driven metal oxide thermochemical cycles. Ind Eng Chem Res 2013;52(9):3276–86.

[34] Smestad Greg P, Steinfeld Aldo. Review: photochemical and thermochemical production of solar fuels from H_2O and CO_2 using metal oxide catalysts. Ind Eng Chem Res 2012;51(37):11828–40.

[35] Steinfeld A. Solar hydrogen production via a two-step water-splitting thermochemical cycle based on Zn/ZnO redox reactions. Int J Hydrogen Energy 2002;27(6):611–9.

[36] Sundell Per G, Björketun Mårten E, Wahnström Göran. Thermodynamics of doping and vacancy formation in $BaZrO_3$ perovskite oxide from density functional calculations. Phys Rev B 2006;73(10):104112.

[37] Tran Fabien, Blaha Peter. Accurate band gaps of semiconductors and insulators with a semilocal exchange-correlation potential. Phys Rev Lett 2009;102(22):226401.

[38] Wang Yanchao, Lv Jian, Zhu Li, Ma Yanming. CALYPSO: a method for crystal structure prediction. Comput Phys Commun 2012;183(10):2063–70.

[39] Wu Qi-Hui, Thissen A, Jaegermann W, Liu Meilin. Photoelectron spectroscopy study of oxygen vacancy on vanadium oxides surface. Appl Surf Sci 2004;236(1–4):473–8.

[40] Yang Chih-Kai, Yamazaki Yoshihiro, Aydin Aykut, Haile Sossina M. Thermodynamic and kinetic assessments of strontium-doped lanthanum manganite perovskites for two-step thermochemical water splitting. J Mater Chem A 2014;2(33):13612–23.

[41] Yang Zongxian, Luo Gaixia, Lu Zhansheng, Hermansson Kersti. Oxygen vacancy formation energy in Pd-doped ceria: a DFT+*U* study. J Chem Phys 2007;127(7):074704.

[42] Youssef Mostafa, Yildiz Bilge. Intrinsic point-defect equilibria in tetragonal ZrO_2: density functional theory analysis with finite-temperature effects. Phys Rev B 2012;86(14):104109.